

Magnetic Monopole Noise

Ritika Dusad^{1†}, Franziska K.K. Kirschner^{2†}, Jesse C. Hoke^{1,3}, Benjamin Roberts¹, Anna Eyal^{1,4}, Felix Flicker⁵, Graeme M. Luke^{6,7,8}, Stephen J. Blundell² and J.C. Séamus Davis^{1,2,9}

1. *Department of Physics, Cornell University, Ithaca, NY 14853, USA.*
 2. *Clarendon Laboratory, Oxford University, Parks Road, Oxford, UK*
 3. *Department of Physics, Stanford University, Stanford, CA 94305, USA*
 4. *Department of Physics, Technion – Israel Institute of Technology, Haifa, 3200003, Israel*
 5. *Rudolf Peierls Centre for Theoretical Physics, Clarendon Laboratory, Parks Road, Oxford, UK*
 6. *Brockhouse Inst. for Materials Research, McMaster University, Hamilton, ON, Canada.*
 7. *Department of Physics, McMaster University, Hamilton, Ontario, L8S 4M1, Canada.*
 8. *Canadian Institute for Advanced Research, Toronto, Ontario, M5G 1Z8, Canada.*
 9. *Department of Physics, University College Cork, Cork T12R5C, Ireland.*
- † Contributed equally to this project.

ABSTRACT Magnetic monopoles¹⁻³ are hypothetical elementary particles exhibiting quantized magnetic charge $m_0 = \pm(h/\mu_0 e)$ and quantized magnetic flux $\Phi_0 = \pm h/e$. A classic proposal for detecting such magnetic charges is to measure the quantized jump in magnetic flux Φ threading the loop of a superconducting quantum interference device (SQUID) when a monopole passes through it⁴. Naturally, with the theoretical discovery that a plasma of emergent magnetic charges should exist in several lanthanide-pyrochlore magnetic insulators^{5,6} including $\text{Dy}_2\text{Ti}_2\text{O}_7$, this SQUID technique was proposed for their direct detection⁶. Experimentally, this has proven extremely challenging because of the high number density, and the generation-recombination (GR) fluctuations, of the monopole plasma. Recently, however, theoretical advances have allowed the spectral density of magnetic-flux noise $S_\Phi(\omega, T)$ due to GR fluctuations of $\pm m_*$ magnetic charge pairs to be determined^{7,8}. These theories present a sequence of strikingly clear predictions for the magnetic-flux noise signature of emergent magnetic monopoles. Here we report development of a high-sensitivity, SQUID based flux-noise spectrometer, and consequent measurements of the frequency and temperature dependence of $S_\Phi(\omega, T)$ for $\text{Dy}_2\text{Ti}_2\text{O}_7$ samples. Virtually all the elements of $S_\Phi(\omega, T)$ predicted for a magnetic monopole plasma,

including the existence of intense magnetization noise and its characteristic frequency and temperature dependence, are detected directly. Moreover, comparisons of simulated and measured correlation functions $C_\Phi(t)$ of the magnetic-flux noise $\Phi(t)$ imply that the motion of magnetic charges is strongly correlated because traversal of the same trajectory by two magnetic charges of same sign is forbidden. A final striking observation is that, since the GR time constants $\tau(T)$ are in the millisecond range for $\text{Dy}_2\text{Ti}_2\text{O}_7$, magnetic monopole flux noise amplified by the SQUID is audible to human perception.

Observation of a quantized jump in magnetic flux Φ threading a SQUID loop when a monopole passes through it is a technique designed for direct detection of magnetic monopoles⁴. This is because, if a magnetic charge m_0 travels from $x = -\infty$ to $x = +\infty$ through the SQUID input loop, the net flux from the radial magnetic field $|\mathbf{B}(\mathbf{r})| = \mu_0 m_0 / 4\pi r^2$ changes continuously from 0 to Φ_0 (Fig. 1A). This technique was proposed⁶ for the direct detection of emergent magnetic charges in magnetically-frustrated lanthanide-pyrochlore insulators^{9,10} such as $\text{Dy}_2\text{Ti}_2\text{O}_7$ and $\text{Ho}_2\text{Ti}_2\text{O}_7$. In these materials, pairs of magnetic charges $\pm m_*$ are generated by thermal activation and, if each charge departs to $\pm\infty$ in opposite directions, the net flux threading the SQUID loop should evolve from 0 to $\Phi_* = m_* \mu_0$ (Fig. 1B). However, because these materials are hypothesized to contain a dense plasma of equal numbers of $\pm m_*$ magnetic charges that are undergoing rapid thermal generation and recombination, $\Phi(t)$ measured by a SQUID (Fig. 1C) is expected to be stochastic, weak, and with zero-average. Therefore, although there is much indirect evidence for the existence of the magnetic charge plasma in $\text{Dy}_2\text{Ti}_2\text{O}_7$ and $\text{Ho}_2\text{Ti}_2\text{O}_7$ (Ref. 9,10), the magnetic-flux signature⁶ of the emergent magnetic charges m_* has so far gone undetected.

In these compounds, the rare-earth magnetic ions ($\text{Dy}^{3+}; \text{Ho}^{3+}$) sit on a sublattice of corner-sharing tetrahedra (Fig. 1D). They have only two low energy spin configurations in the form of an Ising magnetic moment ($\mu \approx 10\mu_B$) that points either towards or away from

the center of each tetrahedron^{9,11} (black arrows Fig. 1D). The nearest-neighbor interaction between these Ising moments⁹ takes the form $-J\sum \mathbf{S}_i \cdot \mathbf{S}_j$, with $J \approx -3.7\text{K}$ for $\text{Dy}_2\text{Ti}_2\text{O}_7$ and $J \approx -1.6\text{K}$ for $\text{Ho}_2\text{Ti}_2\text{O}_7$. Out of a possible 16, this interaction selects 6 energetically degenerate ground state spin configurations¹² on a tetrahedron, all having two spins pointing in and two pointing out (2in/2out) as shown in Fig. 1D. The resulting classical Hamiltonian is labelled the dipolar spin ice (DSI) model, and incorporates both these nearest-neighbor exchange interactions and longer range dipole interactions in the form¹³

$$H = -J \sum_{\langle i,j \rangle} \mathbf{S}_i \cdot \mathbf{S}_j + Da^3 \sum_{i < j} \left[(\mathbf{S}_i \cdot \mathbf{S}_j) / |r_{ij}|^3 - \frac{3(\mathbf{S}_i \cdot \mathbf{r}_{ij})(\mathbf{S}_j \cdot \mathbf{r}_{ij})}{|r_{ij}|^5} \right] \quad (1).$$

Here $D = \mu_0 \mu^2 / (4\pi a^3)$ is the dipole-interaction energy scale $D \approx +1.41\text{K}$ for both $\text{Dy}_2\text{Ti}_2\text{O}_7$ and $\text{Ho}_2\text{Ti}_2\text{O}_7$, and $a=0.354\text{ nm}$ is the nearest-neighbor distance between moments. The magnetic monopole model of the spin ices is achieved by re-writing the real Ising dipoles $\pm\mu$ of Eq. (1) in terms of magnetic charges $\pm m_*$ placed at the centers of adjacent tetrahedra such that $\pm\mu = \pm m_* d/2$ (Fig. 1D) where d is the distance between tetrahedron centers r_α . Each center r_α is then labeled by a net magnetic charge m_α : $m_\alpha=0$ for 2-in/2-out, $m_\alpha = m_*$ for 3-out/1-in and $m_\alpha = -m_*$ for 3-in/1-out configurations (Fig. 1D). The interaction potential between such magnetic charges m_α and m_β at sites r_α and r_β is then represented by the Hamiltonian^{6,9}

$$H = \frac{\mu_0}{4\pi} \sum_{\alpha < \beta} \frac{m_\alpha m_\beta}{r_{\alpha\beta}} + \frac{\nu}{2} \sum_{\alpha} m_\alpha^2 \quad (2)$$

with $\nu = J/3 + 4/3 (1 + \sqrt{\frac{2}{3}})D$. Here the first term represents the Coulomb-like interactions between magnetic charges, and the second an on-site repulsion which enforces the $m_\alpha=0$ or 2-in/2-out ground state at $T=0$. In this picture, when thermal fluctuations randomly flip a fraction of the Dy spins, this generates a plasma of emergent monopole quasiparticles with magnetic charges $\pm m_*$, plus a small additional population¹⁴ with charge $\pm 2m_*$. Overall, the

low-energy spin excitations in DSI materials are hypothesized to be a plasma of $\pm m_*$ magnetic charges^{5,6,9,10}, that are interacting via a Coulomb-like potential, while undergoing rapid thermally activated generation and recombination across an energy barrier $\Delta \approx 2v(\mu/d)^2$.

Thermally generated plasmas of $\pm q$ electric charges, subject to both Coulomb interactions and rapid spontaneous generation and recombination, are well known and understood in intrinsic semiconductors¹⁵⁻¹⁹. Here, thermal generation and recombination (GR) of $\pm q$ pairs generates a spectral density of voltage noise $S_V(\omega, T) = V^2 S_N(\omega, T)/N_0^2$, where $S_N(\omega, T)$ is the spectral density of generation-recombination fluctuations in the number of $\pm q$ pairs, and N_0 is their equilibrium density at a given temperature T . Analogous theories for generation-recombination fluctuations within a plasma of $\pm m_*$ magnetic-charge pairs have very recently been developed for spin ice compounds⁷. The rates of $\pm m_*$ pair generation $g(N, T)$ and recombination $r(N, T)$ are such that, $g(N, T)|_{N_0} = r(N, T)|_{N_0}$ where $N_0(T)$ is the equilibrium number of magnetic charge pairs. However, thermally stimulated fluctuations δN in the number of $\pm m_*$ pairs about the equilibrium value N_0 must also occur due to the generation and recombination processes. The Langevin Equation for these magnetic charge number fluctuations has been derived⁷

$$\frac{d(\delta N)}{dt} = -\frac{\delta N}{\tau(T)} + \sqrt{A}\zeta(t) \quad (3)$$

where the GR rate is $1/\tau(T) = \frac{d(r-g)}{dN}|_{N_0}$ i.e. the difference in between rates of charge of recombination and generation taken at N_0 , $A = 2g(N_0)/N_0^2$, and $\zeta(t)$ represents the thermally generated stimulus uncorrelated in time^{7,14}. Taking the Fourier transform of Eqn. 3 yields the predicted spectral density of $\pm m_*$ pair fluctuations as⁷

$$S_N(\omega, T) = \frac{4\sigma_N^2\tau(T)}{(1+\omega^2\tau^2(T))} \quad (4)$$

where $\sigma_N^2 \equiv \overline{(N - N_0)^2}$ is the variance in the number of $\pm m_*$ pairs. This result, shown schematically in Fig. 2A for a sequence of different $\tau(T)$, reveals many intriguing properties. The spectral density of $\pm m_*$ pair fluctuations should be constant up to an angular frequency $\omega_{GR}(T) \sim 1/\tau_{GR}(T)$ on the so-called GR noise plateau, which occurs because of the pure randomness of the magnetic charge GR processes. Above this frequency, $S_N(\omega, T)$ should eventually fall off as $1/\omega^2$ in the range of time scales for which the uncorrelated magnetic charges are propagating freely. Another key signature from Eqn. 4 of the magnetic charge GR processes would be that, in a regime where σ_N^2 is approximately constant⁷, the power spectral density of lowest frequency number fluctuations $S_N(\omega \rightarrow 0, T)$ should increase proportionate to $\tau(T)$.

However, there remains a key challenge to SQUID detection of emergent magnetic monopoles⁶: the GR fluctuations of $\pm m_*$ pairs $S_N(\omega, T)$ must be related directly to fluctuations $S_\phi(\omega, T)$ of magnetic flux $\Phi(t)$ detectable by a SQUID (Fig. 1C). Moreover, Eqn. 4 does not account for correlations in the motion of singly charged monopoles, nor for the existence of any doubly charged monopoles¹⁴. The correlations are theorized to exist due to the special topological constraints in spin ice, which distinguish the dynamics of $\pm m_*$ pairs in these materials from simple particle-antiparticle pairs in free space. Monopoles of opposite signs are connected by a Dirac string with magnetic flux $\Phi_* = m_* \mu_0$ (yellow trace Fig 1D), and its existence renders sequential traversal of the same trajectory by two magnetic charges of same sign as forbidden¹⁰. Therefore, a microscopic theory for magnetization fluctuations and noise, including the effects of both doubly-charged monopoles and correlated monopole motion, is required. Here we use Monte Carlo (MC) simulations of the thermally generated magnetic configurations from Eqn. 1 (SI Section A), with the correspondence between the MC time-step and seconds established as described in SI Section E. The result is a prediction of the spectral density of fluctuations $S_{M_z}(\omega, T)$ in the z-component of magnetization for each ω and T in $\text{Dy}_2\text{Ti}_2\text{O}_7$. These MC simulation-data are

shown in Fig. 2B as the noise spectral density of magnetic field fluctuations $S_{B_Z}(\omega, T)$ for $\text{Dy}_2\text{Ti}_2\text{O}_7$ crystals of approximately our sample volume. Because our specific samples are $\approx 10^{16}$ larger in volume than what is now possible to study by MC simulations, the absolute magnitude of $S_{B_Z}(\omega, T)$ is merely an estimation (SI Section A). This approximation occurs because the effects of finite-size scaling on the DSI MC simulations²⁰ are unknown over the volume range used here, and numerical methods to achieve accurate MC simulations of spin dynamics in a millimeter-size sample of $\text{Dy}_2\text{Ti}_2\text{O}_7$ are an outstanding challenge. Nevertheless, these MC predictions contain several remarkable features. First, the analytic form of $S_{B_Z}(\omega, T)$ revealed by MC studies (Fig. 2B) is equivalent in its key characteristics to Eqn. 4 (Fig. 2A) as derived using the Langevin Eqn. for GR fluctuations of $\pm m_*$ pairs. Second, when MC-simulation of $S_{B_Z}(0, T)$ is plotted versus $\tau(T)$ for the temperature range of our experiments (Fig. 2C), they are approximately proportional, once an offset to all values of $S_{B_Z}(0, T)$ due to numerical Nyquist (sampling) noise is considered. Third, by fitting the functional form $\tau(T)/(1 + (\omega\tau(T))^b)$ to the MC-simulation data in Fig. 2B, one can determine $\tau(T)$. Here the simple relationship $S(\omega) \propto \omega^{-2}$ at high frequencies from GR theory with a single microscopic time constant, is replaced with a more nuanced behavior $S(\omega) \propto \omega^{-b}$ with $b(T) < 2$, possibly due to a combination of spectra as in Eqn. 4 with a distribution of time constants. In any case, as discussed below, the MC simulations indicate that this $S(\omega) \propto \omega^{-b}$ behavior in $\text{Dy}_2\text{Ti}_2\text{O}_7$ derives microscopically from topological constraints on the Dirac strings (2-in-2-out constraints prevent two magnetic charges of same sign from sequentially following the same trajectory) causing the motion of monopoles to become correlated.

These theoretical innovations provide new perspectives on the challenge of detecting the magnetic-flux signature of emergent magnetic monopoles⁶. A sequence of clear predictors emerges for the magnetic-flux noise spectral density $S_\Phi(\omega, T)$ due to a plasma of $\pm m_*$ magnetic charges undergoing GR processes. First, random fluctuations dominate at

frequencies $\omega\tau(T) \ll 1$ and topologically constrained monopole dynamics dominate at $\omega\tau(T) \gg 1$, with a transition regime surrounding $\omega\tau(T) \approx 1$. Second, even though the evolution with T of magnetic charge recombination times $\tau(T)$ is microscopically complex¹⁰, the GR prediction for a plasma of $\pm m_*$ magnetic charges is that

$$S_\phi(0, T) \propto \tau(T) \quad (5)$$

provided that σ_N^2 remains approximately constant in the temperature range of the experiment (Ref. 7 and SI Section B). Third, the signatures of topological constraints on the interactions between monopoles are contained within the prediction⁸ for the magnetic-flux noise autocorrelation function $C_{B_Z}(t)$ and power-law $b(T)$. These concepts are embodied in the predictions that $S_\phi(\omega, T)$ takes the form

$$S_\phi(\omega, T) \propto \tau(T)/[1 + (\omega\tau(T))^b] \quad (6)$$

To exploit these opportunities, we developed a high-sensitivity SQUID based flux-noise spectrometer^{21,22} to measure $S_\phi(\omega)$ generated by crystalline samples. Here we use it for determination of $S_\phi(\omega, T)$ from $\text{Dy}_2\text{Ti}_2\text{O}_7$ samples over a frequency range $1\text{Hz} < f < 2.5\text{kHz}$ (SI Section C). This spin-noise spectrometer (SNS) is mounted on a custom-built, low-vibration, variable temperature cryostat operable in the range $1.2\text{K} \leq T \leq 7\text{K}$, which was estimated to be optimal for detection of most intense noise spectra in $\text{Dy}_2\text{Ti}_2\text{O}_7$. The samples and superconducting circuitry are contained within a cylindrical superconducting Nb shield to suppress external flux noise at the NbTi pickup coil, achieving an operating noise floor of $\sim 4\mu\phi_0/\sqrt{\text{Hz}}$. The primary coil consists of six turns of fine NbTi wire of diameter = 0.09mm, closely wound on the cylindrical MACOR shell (Fig. 1C). We study single crystals of $\text{Dy}_2\text{Ti}_2\text{O}_7$ grown by floating zone techniques, cut in the shape of a rod, and then inserted along the axis of the pickup coil. The superconducting pickup coil makes a persistent connection via two fine NbTi wires to the input coil of a Quantum Design 550 DC SQUID. Measurements then consist of varying the temperature of the SQUID and sample assembly, from 1.2K to 4K in steps of 25mK, and measuring the flux noise spectral density $S_\phi(\omega, T)$ generated by

$\text{Dy}_2\text{Ti}_2\text{O}_7$ samples throughout this temperature range. The output of the SQUID is sent directly to a spectrum analyzer set to record noise spectral density. For these measurements, five datasets are recorded at each temperature in a bandwidth (BW) of 2.5kHz; each dataset itself is the result of averaging of 1000 acquisitions of the spectrum to optimize the signal-to-noise ratio of the noise spectral density measurement at $\sim 100:1$.

Figure 3A shows a typical example of $S_\phi(\omega, T)$ measured from $\text{Dy}_2\text{Ti}_2\text{O}_7$ samples in our SNS apparatus for temperatures in the range $1.2\text{K} \leq T \leq 4\text{K}$. The left-hand axis is the measured magnetic-flux noise spectral density $S_\phi(\omega, T)$ while the right-hand axis shows an estimate of the equivalent magnetic-field noise spectral density $S_{B_z}(\omega, T)$ within the $\text{Dy}_2\text{Ti}_2\text{O}_7$ samples, with the calibration procedure described in SI Section C. Each data set is fit to Eq. (6) with the best fit shown as a fine solid curve. The fit quality is excellent throughout, with the R^2 of all fits exceeding 0.99 (SI Section D). Thus, we find that the magnetic-flux noise spectral density of $\text{Dy}_2\text{Ti}_2\text{O}_7$ is constant for frequencies from near 1Hz up to an angular frequency $\omega(T) \sim 1/\tau(T)$, above which it falls off as ω^{-b} where b spans a range between 1.2 and 1.5. In Fig. 3B we present data from the same magnetic-flux noise measurement, now in the normalized form $S_\phi(\omega, T)/S_\phi(0, T)$, showing directly how the time constant $\tau(T)$ evolves rapidly toward longer times at lower T . An intriguing observation is that, since the monopole times $\tau(T)$ are in the millisecond range, magnetic monopole flux noise amplified by the SQUID is audible to human perception (audio files attached). Finally, Fig. 3C shows the measured $S_\phi(0, T)$ from 3A plotted against the measured $\tau(T)$ from fits in 3A, where T is the implicit variable ranging from 1.2K to 4K. Thus, $S_\phi(0, T)$ of $\text{Dy}_2\text{Ti}_2\text{O}_7$ is proportional to $\tau(T)$ throughout our temperature range, as expected (Fig. 2C), so that the low frequency flux-noise spectral density $S_\phi(0, T)$ rises with falling temperature (Fig. 4A). This situating is expected within GR models when the variance in monopole number σ_N^2 remains roughly constant, experimental confirmation for which is given in SI Section D. Moreover, comparison of $\tau(T)$ derived here from flux-noise spectroscopy data and $\tau(T)$

derived from traditional magnetic susceptibility measurements, reveal them to have good correspondence of temperature dependences²³⁻²⁷ where common data exist (SI Section D). Most generally, all the magnetic-flux noise phenomena observed (Fig. 3, 4A) are consistent with the theoretical predictions (Fig. 2) for a thermally generated plasma of $\pm m_*$ magnetic charges that is dominated by generation-recombination fluctuations.

The observed dependence of magnetic-flux noise on frequency contains additional key information. Monte-Carlo simulations for $\text{Dy}_2\text{Ti}_2\text{O}_7$ can directly predict the autocorrelation function $C_{B_Z}(t, T)$ of magnetic field fluctuations $B_Z(t)$ (Ref. 8). Figure 4B shows $\log [C_{B_Z}(t, T)/C_{B_Z}(0, T)]$ predictions for three distinct magnetic charge dynamics theories at $T=1.2\text{K}$. The first MC model (blue) describes $\pm m_*$ magnetic charge plasma of dipolar spin ice (DSI) which has Coulomb-like inter-particle interactions, and in which the existence of a Dirac-string (yellow Fig. 1D) produces strong constraints by preventing another monopole of the same charge from following the same route^{8,10}. The second MC model (green) is the nearest neighbor spin ice model (NNSI) in which Coulomb-like interactions are suppressed but Dirac-string constraints present. The final model (red) is a neutral plasma of $\pm m_*$ magnetic charges with Coulomb interactions present that is topologically unconstrained. For comparison, our measured autocorrelation function $\log [C_{B_Z}(t, T)/C_{B_Z}(0, T)]$ of magnetic-field fluctuations $B_Z(t)$ is plotted in black and with a best-fit curve overlaid. Clearly the DSI model, including Coulomb-like interactions and Dirac-string topological constraints, is far more consistent with the directly measured correlation function in this system. Moreover, the NNSI model with suppressed Coulomb-like interactions, is inconsistent with the experiment, and short time correlations appear to be completely absent. Except for evolution of the time constant $\tau(T)$ with temperature, these correlation phenomena are virtually unchanged within our temperature range. Equivalently, the MC predictions of exponent b for the power-law falloff of magnetic-flux noise from the same three theories DSI (blue), NNSI (green) and free monopoles (red) can be determined by fitting each

simulated $S_{B_Z}(\omega, T)$ to $\tau(T)/(1 + (\omega\tau(T))^{b(T)})$. The results are shown in Fig. 4C with the measured $b(T)$ from fitting to $S_{B_Z}(\omega, T)$ in Fig. 3A shown as black dots. We note that the predictions of GR theory in Eqn. 4 are well supported by these MC simulations, which predict $S_\phi(\omega, T) \propto \tau/(1 + (\omega\tau)^b)$ where $b=2$ for uncorrelated free monopoles and $b<2$ for the full DSI Hamiltonian. Moreover, comparison between simulated and measured autocorrelation functions $C_{B_Z}(t, T)$ and falloff exponents b , for magnetic-flux noise in $\text{Dy}_2\text{Ti}_2\text{O}_7$ reveals that the DSI model is most consistent with the observed phenomenology. To achieve precise agreement may require adjustment of the J, D terms in Eqn. 1 to deal with more complex and longer range spin-spin interactions²⁸. But overall, the data in Fig. 4C imply that the power-law signatures of strong correlations observed in both $\log [C_{B_Z}(t, T)/C_{B_Z}(0, T)]$ and $S_{B_Z}(\omega, t)$ are occurring due to a combination of the existence of a Dirac-string trailing each monopole (Fig. 1D) and the Coulombic interactions.

To recapitulate: by introducing SQUID-based spin noise spectroscopy techniques to studies of lanthanide-pyrochlores, theoretical predictions for the magnetic-flux signature of a $\pm m_*$ magnetic charge plasma^{6,7,8} in spin ice, are studied for the case of $\text{Dy}_2\text{Ti}_2\text{O}_7$. The strong magnetization noise predicted to exist in these specific materials by Monte-Carlo simulations⁸ (Fig. 2) is observed for the first time (Fig. 3A). The frequency and temperature dependence of the magnetic-flux noise spectrum $S_\phi(\omega, T)$ predicted for $\pm m_*$ magnetic charges undergoing thermal generation and recombination (Fig. 2B,C) is confirmed directly and in detail (Fig. 3). The expected transition from a plateau of constant magnetic-flux noise^{7,8} for $\omega\tau(T) \ll 1$, to a power-law falloff⁸ for $\omega\tau(T) \gg 1$, is observed throughout (Fig. 3A). And the low-frequency flux-noise spectral density $S_\phi(0, T)$ increases rapidly with falling T (Fig. 4A). These $S_\phi(\omega, T)$ characteristics are exceptional, in that the magnetization-noise spectral density signature of a ferromagnet²¹, a classic spin glass²², or an Ising paramagnet²⁹ all evolve very differently with ω and T . On the other hand, the observed phenomenology of

$S_\phi(\omega, T)$ in $\text{Dy}_2\text{Ti}_2\text{O}_7$ is quite analogous to that of voltage-noise spectral density from GR of electron-hole pairs in semiconductors^{15,16,18,19,30}. Thus within the context of $\pm m_*$ generation-recombination theory, the flux-noise spectral density $S_\phi(\omega, T)$ (Figs. 3,4) is highly consistent with other studies implying that $\text{Dy}_2\text{Ti}_2\text{O}_7$ and $\text{Ho}_2\text{Ti}_2\text{O}_7$ contain a plasma of emergent magnetic monopoles^{9,10,14,31-36}. Additionally, the agreement of measured magnetization noise autocorrelation functions $C_{B_z}(t)/C_{B_z}(0)$ with those predicted from MC simulations (Fig. 4B), indicates that significant correlations exist in the motions of $\text{Dy}_2\text{Ti}_2\text{O}_7$ magnetic monopoles. Overall, we find detailed and comprehensive agreement between current theories for thermal generation and recombination of a correlated $\pm m_*$ magnetic monopole plasma (Fig. 2) and the phenomenology of magnetic-flux noise spectral density in $\text{Dy}_2\text{Ti}_2\text{O}_7$ (Figs. 3,4) that is revealed by spin-noise spectroscopy.

FIGURES

Figure 1

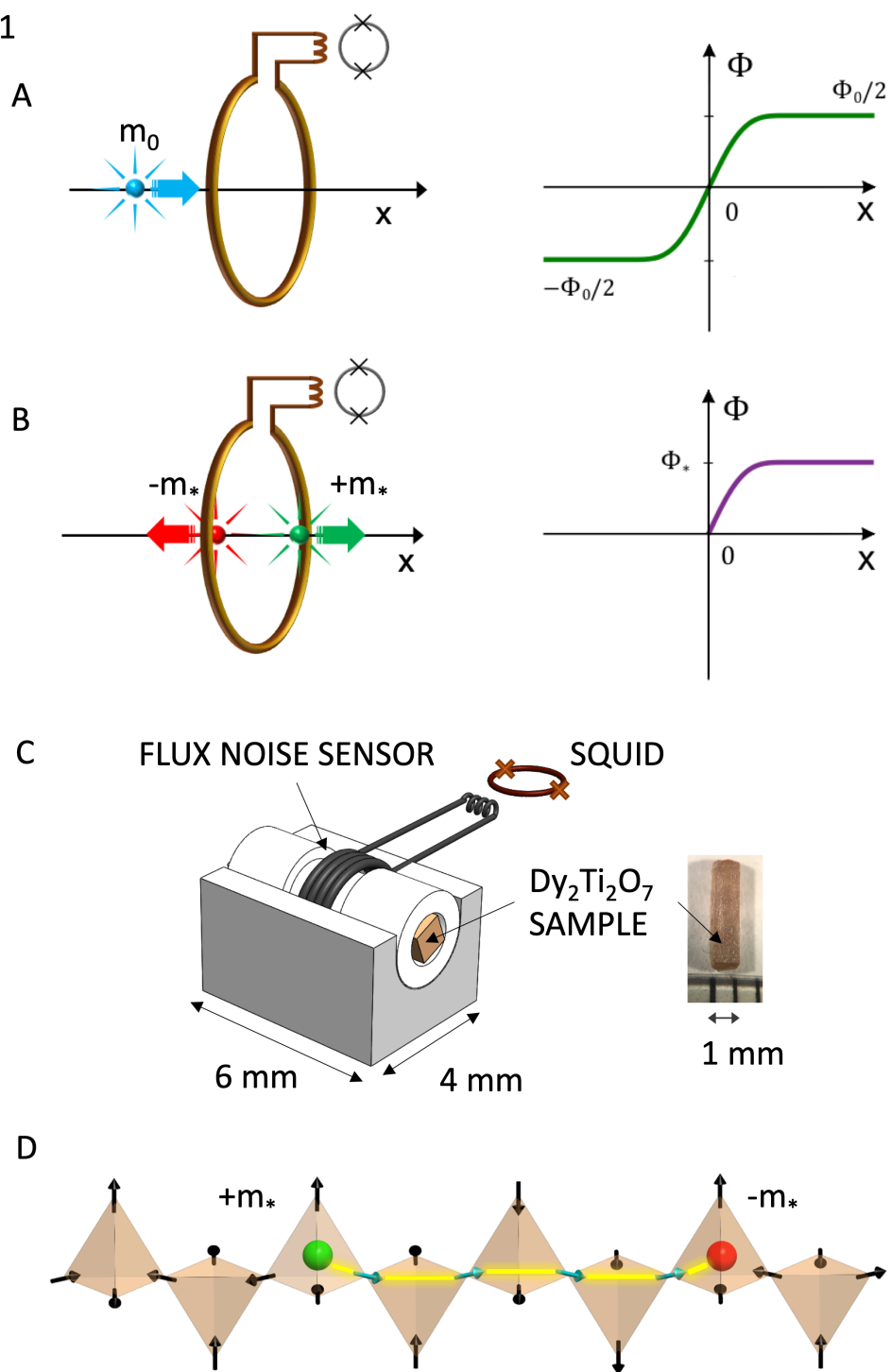


Figure 1 SQUID-based Quantized Flux Jump Detection of Magnetic Monopole

- A. Schematic of fundamental Dirac magnetic monopole with charge m_0 traversing, from $x = -\infty$ to $x = +\infty$, through the input-coil of the SQUID. The magnetic-flux threading the SQUID changes in total by $\Phi_0 = h/e$.
- B. Schematic of two emergent magnetic charges $\pm m_*$ generated in $\text{Dy}_2\text{Ti}_2\text{O}_7$ at $x=0$ by a thermal fluctuation. As each charge departs in opposite directions to $x = \pm\infty$, the net flux threading the SQUID changes in total by $\Phi_* = \mu_0 m_*$.
- C. Schematic of the spin-noise spectrometer used throughout this project (SI Section C). The primary coil, consisting of six turns of 0.09mm diameter NbTi wire wound on the cylindrical MACOR shell, and its two connecting wires to the input coil of a Quantum Design 550 DC SQUID, are contained within a cylindrical superconducting Nb flux shield (not shown). The thermal conductivity of MACOR is sufficient to thermalize the sample for all $T > 1\text{K}$. Inset: single crystals of $\text{Dy}_2\text{Ti}_2\text{O}_7$ cut in the shape of a square-cross-sectional rod (photo) are inserted along the axis of the pickup coil.
- D. Schematic representation of the spin ice excited state in which two magnetic charges $\pm m_*$ are generated by a spin flip, and propagate through the material. In $\text{Dy}_2\text{Ti}_2\text{O}_7$ the tetrahedron corners are the midpoints of the bonds of a diamond lattice defined by the centers r_α of the tetrahedra, and all such bonds point along the local $[111]$ direction. The ratio of the lattice constant of the diamond d and fundamental pyrochlore lattice a is $d = \sqrt{3/2}a$. A single flip of an Ising Dy^{3+} spin converts the 2-in/2-out $m_\alpha = 0$ configuration in adjacent tetrahedra, to a situation with adjacent $m_\alpha = m_*$ for 3-out/1-in in one and $m_\alpha = -m_*$ for 3-in/1-out in the next. These two opposite magnetic charges can then separate via a sequence of spin flips in sequential tetrahedra which leave them all in the 2-in/2-out $m_\alpha = 0$ configuration except at the ends of this chain. However, due to the spin ice constraints the specific path taken, which can be identified with a Dirac string with flux Φ_* , cannot be traversed sequentially by another such magnetic charge of the same sign.

Figure 2

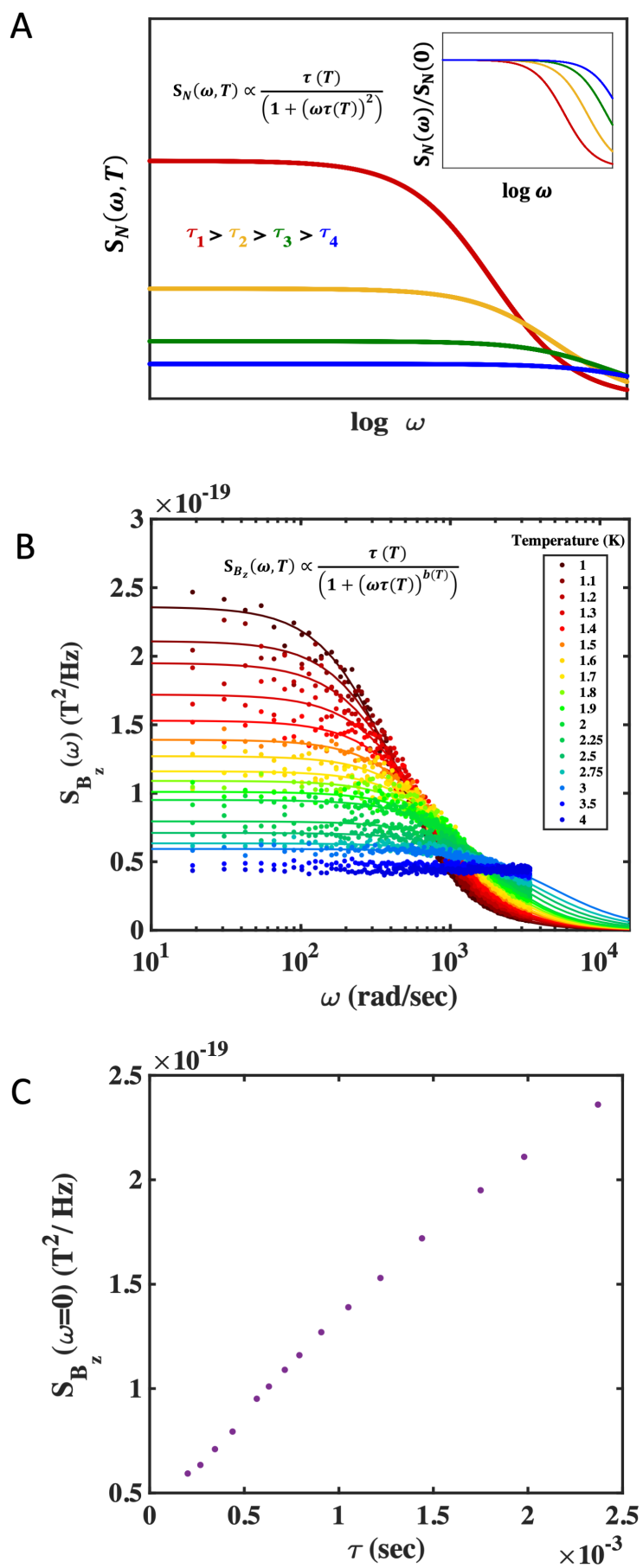
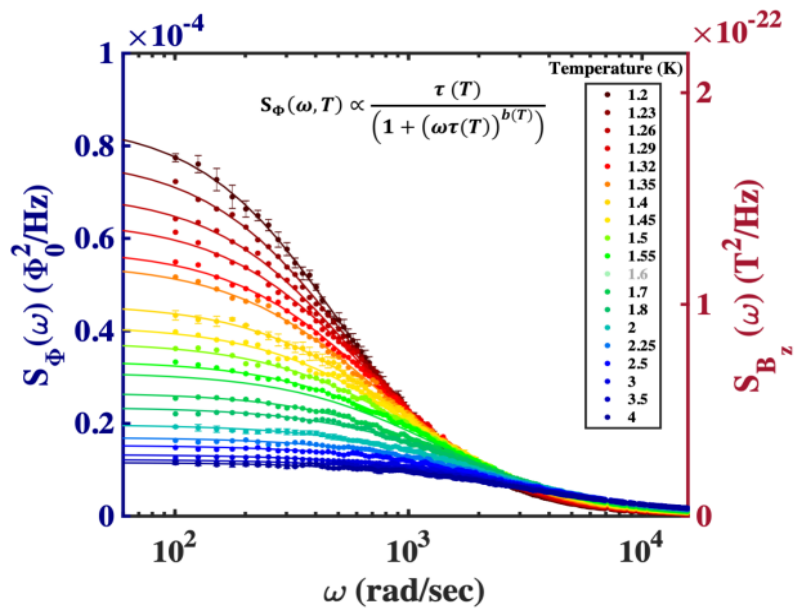


Figure 2 Spectral Density of Fluctuations in Monopole Number and Magnetization

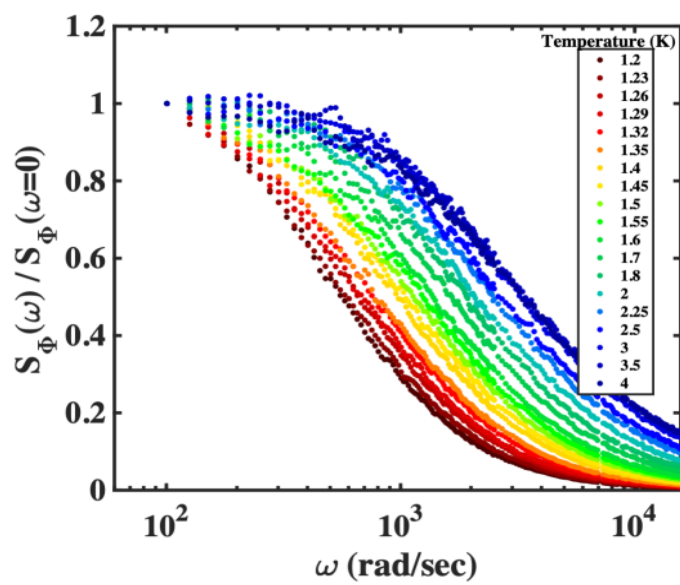
- A. Predicted spectral density of fluctuations in monopole number $S_N(\omega, T)$ from Eqn. 4, for several monopole GR time constants τ , in a range that one might expect to achieve by cooling $\text{Dy}_2\text{Ti}_2\text{O}_7$ from 4K to $\sim 1\text{K}$. The GR plateau in $S_N(\omega, T)$ is clear as $\omega \rightarrow 0$ as is the ω^{-2} falloff expected of free monopole motion for frequencies $\omega\tau > 1$. Top right corner inset shows normalized spectral density $S_N(\omega, T)/S_N(0, T)$. Inset is GR monopole number fluctuation equation $S_N(\omega, T) \propto \tau(T)/(1 + (\omega\tau(T))^2)$.
- B. Predicted spectral density of magnetic field fluctuations within the $\text{Dy}_2\text{Ti}_2\text{O}_7$ sample $S_{B_z}(\omega, T)$ from MC simulations using the Hamiltonian in Eqn. 1 in a range $1\text{K} \leq T \leq 4\text{K}$. Inset is the functional form $S_{B_z}(\omega, T) \propto \tau(T)/(1 + (\omega\tau(T))^{b(T)})$ (see Fig. 4). These simulations are physically quite distinct from those reported in Ref. 8 because here we focus on bulk fluctuations of the z-component of magnetization $M_z(t)$ or of z-component of magnetic field $B_z(t)$, while Ref. 8 considers field fluctuations in vacuum outside a specific crystal termination surface. Because of periodic boundary conditions and the very small MC sample volume, scaling of the predicted magnitude of $S_{B_z}(\omega, T)$ for the MC sample, to the absolute magnitude expected for an experimental sample of volume $\sim 10^{16}$ greater is an approximation (SI Section A). But this in no way affects the form of $S_{B_z}(\omega, T)$ expected for a macroscopic experimental sample.
- C. Predicted relationship from $\text{Dy}_2\text{Ti}_2\text{O}_7$ MC simulations⁸ of $B_z(t)$, of $S_{B_z}(0, T)$ versus $\tau(T)$ for the GR fluctuations of a $\pm m_*$ magnetic charge plasma. Note that all $S_{B_z}(0, T)$ are offset by a constant along the y-axis due to artifacts of Nyquist (sampling) noise at the high frequency end of the MC calculations

Figure 3

A



B



C

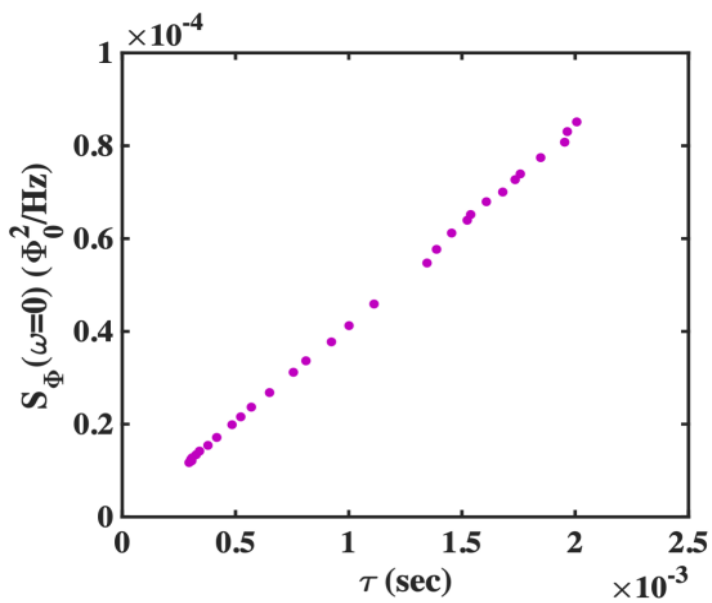


Figure 3 Spectral Density of Magnetic-Flux Noise in Dy₂Ti₂O₇

- A. Measured spectral density of flux-noise $S_\phi(\omega, T)$ from Dy₂Ti₂O₇ samples (e.g. Fig. 1C) in the range $1.2\text{K} \leq T \leq 4\text{K}$. The left-hand axis is the magnetic-flux noise spectral density $S_\phi(\omega, T)$; the right-hand axis is an estimate of the equivalent magnetic-field noise spectral density $S_{B_z}(\omega, T)$ averaged over the Dy₂Ti₂O₇ samples (based on calibration of the flux sensitivity of the spectrometer SI Section C). The best fit to the function $\tau(T)/(1 + (\omega\tau(T))^{b(T)})$ shown as a fine solid curve. Overall we find $S_\phi(\omega, T)$ of Dy₂Ti₂O₇ to be constant for frequencies $1\text{Hz} < (T) = 1/2\pi\tau(T)$, above which it falls off as ω^b .
- B. Normalized spectral density of flux noise $S_\phi(\omega, T)/S_\phi(0, T)$ revealing the divergence of the time constant $\tau(T)$ toward longer times at lower T (SI Fig. 5)
- C. $S_\phi(0, T)$ plotted versus $\tau(T)$ as measured from fitting data in 3A. Observation that $S_\phi(0, T) \propto \tau(T)$ for Dy₂Ti₂O₇ throughout the full temperature range is a key expectation for $\pm m_*$ GR magnetic-flux noise.

Figure 4

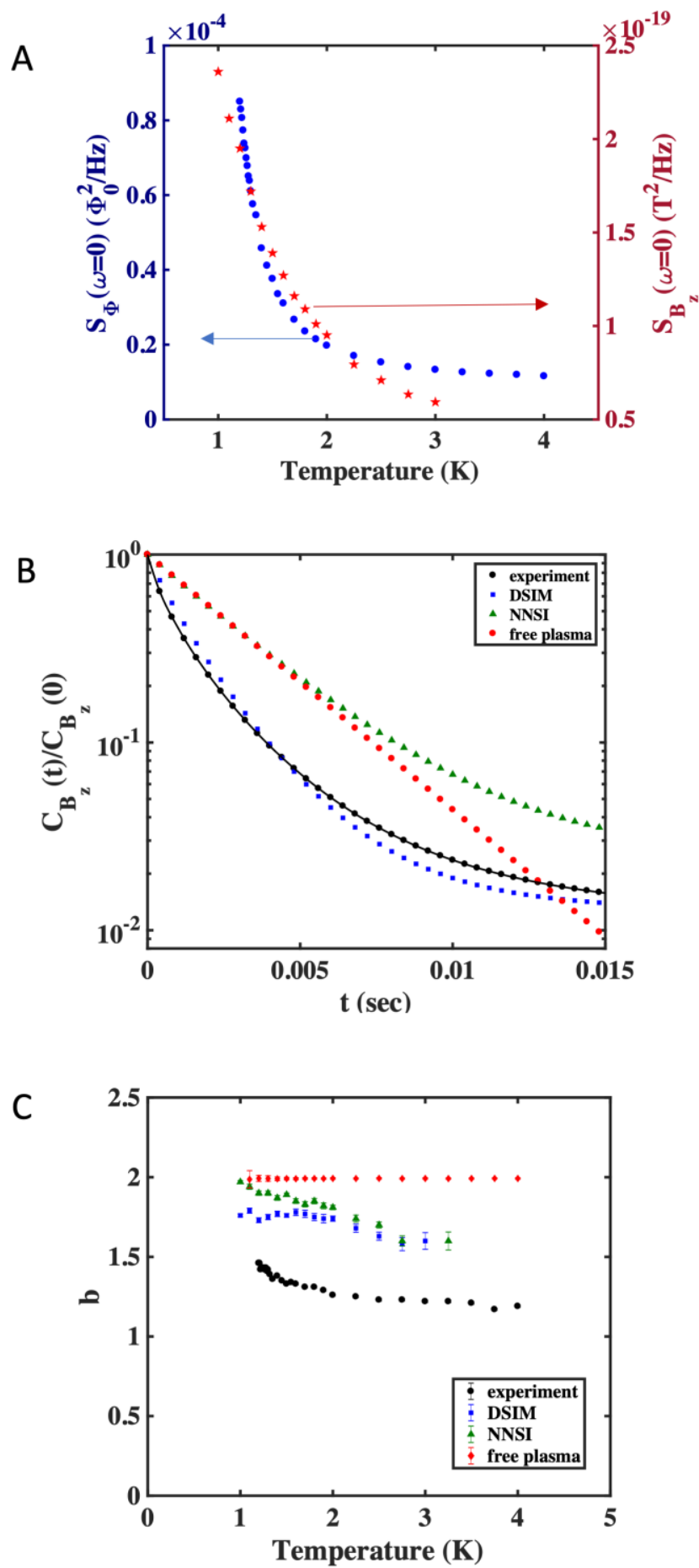


Figure 4 Magnetic Flux Noise Spectral Density of Correlated Monopole Fluid

- A. Experimentally measured $S_\phi(0, T)$ (blue) and MC predicted $S_{B_Z}(0, T)$ low frequency noise spectral density of $\text{Dy}_2\text{Ti}_2\text{O}_7$ with falling temperature.
- B. For $T=1.2\text{K}$, the Monte-Carlo simulation prediction of the autocorrelation function $\log \left[\frac{C_{B_Z}(t)}{C_{B_Z}(0)} \right]$ in the field fluctuations $B_Z(t)$ for three models of the spin dynamics of $\text{Dy}_2\text{Ti}_2\text{O}_7$. The DSI model contains Coulomb-like interactions and constraints on repeated passage of a same-sign monopoles along the same trajectory due to Dirac strings (green); the nearest neighbor spin ice model (NNSI) has had the Coulomb interactions suppressed (blue); the free monopole plasma (red) is in-keeping with free monopole GR theory. The measured autocorrelation function $\log \left[\frac{C_{B_Z}(t)}{C_{B_Z}(0)} \right]$ of magnetic-field fluctuations $B_Z(t)$ of $\text{Dy}_2\text{Ti}_2\text{O}_7$ is plotted in black and overlaid with a fit function; the experimental error bars are smaller than the data points. Clearly the autocorrelation function of the DSI model corresponds best to the measured $C_{B_Z}(t)$. We note that the distinction between the single slope (red) for the free monopole plasma⁷, and the more complex predicted $C_{B_Z}(t)$ for the other cases, represents microscopically a distinction between a simple process involving a single time constant vs. a more complex one, potentially involving a spread of relaxation time constants. Most importantly, the measured $C_{B_Z}(t)$ (black) shows that magnetization dynamics is obviously strongly correlated in time.
- C. Monte-Carlo prediction of exponent b in $S_{B_Z}(\omega, T) \propto \tau(T)/(1 + (\omega\tau(T))^{b(T)})$ for the three magnetic charge dynamics theories. As in B, these are the DSI model (blue); the NNSI model (green); the free plasma model (red). Measured exponent b from fitting $S_\phi(\omega, T) \propto \tau(T)/(1 + (\omega\tau(T))^{b(T)})$ for all data in Fig. 3A is shown in black. The time constants $\tau(T)$ of the MC $S_{B_Z}(\omega, T)$ and of the $S_\phi(\omega, T)$ data are not free parameters here (Fig 4A).

Acknowledgements: We are grateful to C. Castelnovo, J. Goff, Yong Beak Kim, M.J. Lawler, A. Ramirez and N. Y. Yao for very helpful discussions and communications. J.C.S.D. thanks Owen H.S. Davis for insightful discussions and for proposing to study magnetic noise in pyrochlores. R.D. thanks Y.X. Chong for extensive aid during experimental operations. R.D. acknowledges use of technical facilities at Cornell Center for Materials Research Shared Facilities which are supported through the NSF MRSEC program (DMR-1719875). A.E. acknowledges support from the Israeli Pazy Equipment Grant 299/18. F.K.K.K. acknowledges support from Lincoln College, Oxford. F.F. acknowledges support from the Astor Junior Research Fellowship of New College, Oxford. J.C.S.D. acknowledges salary support from the European Research Council (ERC) under the mVITO Project, Grant # DLV-788932. Conceptual design of the experimental technology was supported by the W.M. Keck Foundation. Experimental studies and support for R.D. were funded by the Gordon and Betty Moore Foundation's EPiQS Initiative through Grant GBMF4544.

Author Contributions: R.D. and J.C.S.D. conceptualized the project and designed the experimental setup. R.D. developed the flux noise spectrometer. R.D., J.C.H., B.R. and A.E. carried out the experiments and data analysis. G.M.L. synthesized the sequence of $\text{Dy}_2\text{Ti}_2\text{O}_7$ samples. F.K.K.K. carried out the Monte Carlo simulations with help from F.F. G.M.L., S.J.B. and J.C.S.D. supervised the investigation and wrote the paper with key contributions from R.D., F.K.K.K. and F.F. The manuscript reflects the contributions of all authors.

Supplementary Information

A *Monte Carlo Simulations*

A.1. *MC Simulation Procedures*

Monte Carlo (MC) simulations are used to model the magnetization dynamics of $\text{Dy}_2\text{Ti}_2\text{O}_7$. In general, these simulations were carried out on a sample containing $4 \times 4 \times 4$ unit cells, each of which contains 16 Dy^{3+} ions. We refer to this as the MC sample. Standard MC procedures are used [19], consisting of 10^6 cooling steps followed by an interval of 5000 MC-time-steps, at fixed T . During this interval W , the time dependence of net z-component of magnetic moment $\mu_z(t)$ of the whole MC sample is then simulated. This procedure is then repeated 600 times. Carrying out the MC simulations for 5000 MC sequential time-steps ensures capture of a spread of microscopic time-scales at each temperature which covers that expected in this material at these temperatures. This is because it spans the range from approximately a single MC step $\sim 100\mu\text{s}$ to approximately the total time for which simulation runs $\sim 1\text{s}$. The range of temperatures of these simulations was between 4.0K and 1 K. Because this is a simulation of bulk magnetization dynamics, periodic boundary conditions were used in all directions.

For a given conformation, the z-component of magnetic moment of the MC sample μ_z was found by summing z-components over the individual magnetic moments of the 1024 Dy spins, where $\mu \approx 10\mu_B$. The simulated time dependence of this value at a given temperature T is $\mu_z(t, T)$, and is evaluated sequentially during the time window W . Its autocorrelation function is

$$C_{\mu_z}(\tau, T) = \frac{1}{W} \int_{-W/2}^{W/2} \mu_z(t, T) \mu_z(t + \tau, T) dt \quad [\mu_B^2] \quad (\text{M.1})$$

The predicted spectral density of magnetic moment noise in the MC sample is then calculated using the Wiener-Khinchin theorem

$$S_{\mu_z}(\omega, T) = 4 \int_0^\infty C_{\mu_z}(\tau, T) \cos(\omega\tau) d\tau \quad [\mu_B^2 \text{ MCstep}] \quad (\text{M.2}).$$

We extract the frequency range $10^{-4}(\text{MC-steps})^{-1}$ to $10^{-1}(\text{MC-steps})^{-1}$ (the Nyquist frequency is $0.5(\text{MC steps})^{-1}$). Equation M.2 was then averaged over the 600 independent simulation runs to get better precision for $S_{\mu_z}(\omega, T)$. Finally, the time axis of the MC simulation is converted from MC-step to seconds as described in SI Section E, so that angular frequency in Eqn. M.2 and throughout the paper is $\omega(\frac{\text{rad}}{\text{sec}}) = 2\pi/t(\text{sec})$ and $S_{\mu_z}(\omega, T) [\mu_B^2 \text{ s}]$.

To convert to the noise spectral density of the z-component of the magnetization, we use $S_{M_z}(\omega, T) = \frac{\mu_B^2 S_{\mu_z}(\omega, T)}{V^2}$ [$A^2 m^{-2} s$] where $V=6.6 \times 10^{-26} \text{ m}^3$ is the volume of the MC sample. To estimate the predicted spectral density of z-magnetization noise expected from the $\text{Dy}_2\text{Ti}_2\text{O}_7$ experimental sample within range of the SQUID pickup coil (Fig. 1C), we estimate that there are $N= 2.9 \cdot 10^{16} \pm 20\%$ MC samples in the experimental volume, and divide $S_{M_z}(\omega, T)$ by N . The spectral density of fluctuations of z-component of magnetic field $B[\text{Tesla}]$ within the sample is then

$$S_{B_z}(\omega, T) = \mu_0^2 S_{M_z}(\omega, T) [T^2 s] \quad (\text{M.3}).$$

Figure 2B then shows the estimation of $S_{B_z}(\omega, T)$ in the spin noise spectrometer, for our specific sample geometry, from the DSI Hamiltonian (Eqn. 1)

A.2 Model Hamiltonians

First the full dipolar spin ice Hamiltonian (given in Eq. (1) in the main text) is employed. The exchange energy is $J \approx -3.72 \text{ K}$ and the dipolar energy is $D \approx 1.41 \text{ K}$ for DTO. This dipolar spin ice model (DSIM) leads to a lowest energy state of Dy spins pointing into the center or out of the tetrahedron they are sitting on along the local $\langle 111 \rangle$ axes. This state is known as the 2-in-2-out state (Fig. 1D). As previously discussed, the violation of this rule by a spin flip causes generation of a monopole anti-monopole pair with charge $\pm m_*$ or doubly charged pair with charge $\pm 2m_*$ (Ref. 14). The energy of two nearest-neighbor monopoles is 3.06 K , and the energy to create one monopole is $\Delta = 4.35 \text{ K}$. Since the spins sit on tetrahedral corners, magnetic monopole motion is guided by spin flips in a topologically constrained fashion. These monopoles experience a strong coulombic force between the $\pm m_*$ charges as described in Eqn. (2) of the main text.

Second the nearest-neighbor spin ice (NNSI) Hamiltonian is considered. This is executed by setting $D=0$ in Eqn. 1 of main text. It suppresses the effects of long-range coulombic interactions. J is chosen such that the system still has a 2-in/2-out ground state, while having the same density of excitations as DSI at a given temperature. This system still has monopole-like excitations, but greatly reduced force between the monopoles. Thus, we predict the noise spectral density of $\pm m_*$ magnetic charge pairs hopping in the presence of strongly suppressed coulombic interactions.

Third, we identify the noise spectrum of $\pm m_*$ magnetic charge pairs hopping freely in the absence of Coulomb interactions or topological constraints due to the Dirac strings in $\text{Dy}_2\text{Ti}_2\text{O}_7$. The model is specified in Eq. (2) in the main text, with m_* charges located on the sites of a diamond lattice.

B Statistics of monopole number fluctuations

The master equation for generation $g(N, T)$ and recombination $r(N, T)$ of magnetic monopoles [Ref. 7] defines the probability $P(N, T)$ of finding N monopoles at temperature T in a steady state condition

$$\begin{aligned} \frac{dP(N, T)}{dt} &= r(N + \delta N, T)P(N + \delta N, T) + g(N - \delta N, T)P(N - \delta N, T) \\ &\quad - P(N, T)[g(N, T) + r(N, T)] = 0 \end{aligned} \quad (\text{M.4})$$

Here $g(N, T)$ and $r(N, T)$ are the generation and recombination rates of the monopoles and δN is the number of magnetic monopole particles added or removed by a generation or recombination event respectively. We take this $\delta N = 1$ in the following analysis. The exact dependence of g and r on N and T depends on the microscopics of generation and recombination process pertaining to the specific system under investigation. We also note that (Ref. 15,16,17)

$$\frac{d}{dt} \langle \Delta N \rangle = - \left. \frac{d(r-g)}{dN} \right|_{N=N_0} \quad (\text{M.5})$$

where $\Delta N = N - N_0$. The time constant for N to approach its equilibrium value is defined

$$\frac{1}{\tau(T)} \equiv \left. \frac{d(r-g)}{dN} \right|_{N_0} = r'(N_0, T) - g'(N_0, T) \quad (\text{M.6})$$

Obviously, in equilibrium, $g(N_0, T) = r(N_0, T)$.

Expanding $\ln P(N, T)$ about its maximum value $\ln P(N_0, T)$ in a quadratic fashion (Ref. 15,16) yields

$$\left[\frac{\partial^2}{\partial N^2} \ln P(N, T) \right]_{N=N_0} = \frac{g'(N_0, T)}{g(N_0, T)} - \frac{r'(N_0, T)}{r(N_0, T)} \quad (\text{M.7})$$

so that

$$\ln P(N, T) = \ln P(N_0, T) - \frac{1}{2} (N - N_0)^2 \left[\frac{r'(N_0, T)}{r(N_0, T)} - \frac{g'(N_0, T)}{g(N_0, T)} \right] \quad (\text{M.8})$$

Thus the expected Gaussian probability distribution of N about its most probable value N_0 is

$$P(N, T) = P(N_0, T) \exp \left[-(N - N_0)^2 / 2(N - N_0)^2 \right] \quad (\text{M.9})$$

The variance of monopole number $\sigma_N^2 = \overline{(N - N_0)^2}$ is then determined from equations M.7,9 (Ref. 15,16) as

$$\sigma_N^2(T) = \left[\frac{r'(N_0, T)}{r(N_0, T)} - \frac{g'(N_0, T)}{g(N_0, T)} \right]^{-1} = \frac{g(N_0, T)}{r'(N_0, T) - g'(N_0, T)} = g(N_0, T) \cdot \tau(T) \quad (\text{M.10})$$

For emergent magnetic monopoles in $\text{Dy}_2\text{Ti}_2\text{O}_7$, the equilibrium generation rate at temperature T within our range will approximately be $g(N_0, T) \propto \exp(-\Delta/T)$ where Δ = thermal energy barrier since thermal spin flips generate the monopoles. It is established from previous experiments that at these higher temperatures that the time constants are given approximately by $\tau(T) \sim \exp(\Delta/T)$ (Ref. 24). This implies that the variance of magnetic monopole number $\sigma_N^2 \sim \exp\left(\frac{\Delta}{T}\right) \cdot \exp\left(-\frac{\Delta}{T}\right)$ is approximately constant in this temperature range.

C Spin-noise Spectrometer

C.1 Design

We use a custom-built 1K cryostat to carry out our experiments, with the SQUID and the sample-holder (SH) plus their superconducting shielding mounted below and thermalized to the 1K pot refrigerator. The spin noise spectrometer (SNS) setup consists of cylindrical SH with a concentric hole of diameter 1.4 mm and length 5.7 mm is used to encapsulate rod-shaped samples as shown in Fig. 1C. The superconducting pickup coil is wound around the SH and consists of 6 turns of thin Nb wire with inductance $L \approx 0.25 \mu\text{H}$. The input inductance of the QD 550 SQUID is reported by the manufacturer (Quantum Design) to be $\approx 2.0 \mu\text{H}$. The SH and the SQUID circuitry of the SNS are all contained within a Nb tube of aspect ratio $R \sim 4$ for flux shielding. No external cables enter this shielded region, to minimize external noise being picked-up by our detector. This insures that flux-noise floor of this apparatus sits at minimum level quoted by manufacturer $\Phi < 4 \mu\phi_0 / \sqrt{\text{Hz}}$ for the entire temperature range of study as shown in S.I. Figure 1.

C.2. Operation

A typical operation cycle consists of cooling down experiment to 1.2K and then using PID controls to vary temperature from 1.2K to above 4K with temperature stability at each point of 2.5 mK. Once the temperature is stable at a desired set-point, we record the flux noise generated by our sample via a spectrum analyzer. Unprocessed data at each temperature consists of 5 datasets of BW 2.5kHz, each of which is an outcome of averaging of 1000 acquisitions where acquisition time = $(1/\text{resolution BW})$, resulting in the measured SQUID output as voltage noise spectral density detected at the SQUID $S_v(\omega, T)$.

C.3 Calibration

The transfer function C between pickup coil and SQUID is calibrated by driving a small known flux $\Phi_{TEST}(\phi_0)$ via a drive coil (inserted into the pickup coil) through the pickup coil, and recording the corresponding SQUID output voltage V_S . In this case (S.I. Figure 1)-

$$C = \left(\frac{V_S}{0.684} \right) \frac{1}{\Phi_{TEST}(\phi_0)} \quad (\text{M.11}).$$

We find that $C=0.015$. The spectral density of magnetic-flux noise within the sample is obtained

$$S_\Phi(\omega, T) = S_v(\omega, T)/(C^2). \quad (\text{M.12})$$

To relate $S_\Phi(\omega, T)$ to the magnetic field noise spectral density generated within our sample $S_{Bz}(\omega, T)$, we consider the cross-sectional area of the sample $\sigma = 1.4 \times 10^{-6} \text{m}^2 \pm 17\%$ yielding

$$S_{Bz}(\omega, T) = S_\Phi(\omega, T)/(\sigma)^2 [\text{T}^2\text{s}] \quad (\text{M.13}).$$

C.4 Flux-Noise Signal Strength

A typical magnetic-flux noise spectral density from a sample compared to the noise spectral density of an empty pickup coil is shown in S.I. Figure 2 for BW: 1Hz to 2.5kHz. The plateau of flux-noise spectral density from $\text{Dy}_2\text{Ti}_2\text{O}_7$ sits a factor of 1.5×10^6 higher than the noise floor level. Mechanical noise peaks for empty coil flux signal and for $\text{Dy}_2\text{Ti}_2\text{O}_7$ flux signal have been deleted manually. We note that the plateau for flux-noise spectral density signal of monopoles from $\text{Dy}_2\text{Ti}_2\text{O}_7$ goes down to at least 1Hz.

C.5 Sample Geometry Effects

Shape effects could occur in such spin noise measurements. This is because even though we are measuring a cuboidal sample with a coil around the middle, spins at the ends of the sample still contribute partially. Our experiments measure flux through the pickup coil due to the dipole fields from spins in the sample, and the noise is coming fundamentally from spin flips (aka monopole hops). The flux at the pickup coil due to a single spin in the sample depends on where that spin is and which way it is pointing. Some spins are invisible (e.g. spins pointing to a direction in the xy plane) and some have a greater effect, e.g. spins close to, but not at the edge, in or near the plane of the coil, pointing along z. If there is a fluctuation of the magnetic moment of the whole sample, resulting in a net moment, then that would produce a net demagnetization field which all the spins would experience, potentially affecting their dynamics, and that demagnetization field would be shape-dependent.

D. Data Analysis

D.1 Fitting

The flux-noise spectral density floor measured for empty pickup coil in the SNS, i.e. background noise S_{Φ}^{bcg} , is fitted to a smooth polynomial function S_{Φ}^f . Since the noise floor does not vary with temperature, the same function S_{Φ}^f is then subtracted from the measured $\text{Dy}_2\text{Ti}_2\text{O}_7$, $S_{\Phi}^{DT0}(\omega, T)$ for all temperatures, to obtain the reported noise spectral density $S_{\Phi}(\omega, T)$ dataset shown in Fig. 3.

This post processed data is then fit to empirical equation (6) using Least Squares method for a BW of 16Hz-2.5kHz for all temperatures. While the plateau in flux-noise spectral density $S_{\Phi}(\omega, T)$ goes down to at least 1Hz for all temperatures, to optimize data acquisition times to ~ 1 hour per temperature, for all spectra reported in Fig. 3, the lower limit for BW of data for regression analysis is set at 16Hz. The time constant $\tau(T)$, power law for frequency $b(T)$ and $S_{\Phi}(0, T)$ are free parameters in the fitting procedure and fits for all temperatures are of high quality with $R^2 > 0.99$. The residuals for these fits are shown in S.I. Figure 3.

We established that the flux noise spectral density coming from $\text{Dy}_2\text{Ti}_2\text{O}_7$ is repeatable in different single crystals of the material as shown, for a typical example, in S.I. Figure 4.

D.2 Evolution of time constants

It has been established that the microscopic time-constants involved in magnetic dynamics of $\text{Dy}_2\text{Ti}_2\text{O}_7$ diverge with decreasing T (Ref 22,23,24) and are heterogeneous (Ref 25,26). There have been many ac susceptibility measurements of $\text{Dy}_2\text{Ti}_2\text{O}_7$ in different sample shapes ranging from polycrystalline samples (Ref 24) to toroidal single crystals (Ref 25,26). Yaraskavitch *et al* established that the time constant they measured from SQUID based susceptibility measurements of rod shaped samples were in good qualitative agreement with timescales in Snyder *et al* and Matsuhira *et al*. Eyvazov *et al* verified quantitative agreement between $\tau(T)$ from their susceptibility measurements and $\tau(T)$ from Yaraskavitch *et al*.

In S.I. Fig. 5, we show the $\tau(T)$ obtained by fitting the flux-noise spectrum from our experiment. It clearly follows a quantitatively very similar trajectory to the relaxation time measured in ac susceptibility experiments of Eyvazov *et al*. and thus corresponds well with the $\tau(T)$ derived from susceptibility studies cited for this material (Refs. 22,23,24,25,26)

D.2 Variance in magnetic-flux noise

We note that the measured variance of flux σ_Φ^2 is approximately constant as a function of temperature in S.I. Fig. 6. We measure this variance at each temperature by integrating measured monopole flux noise with respect to frequency.

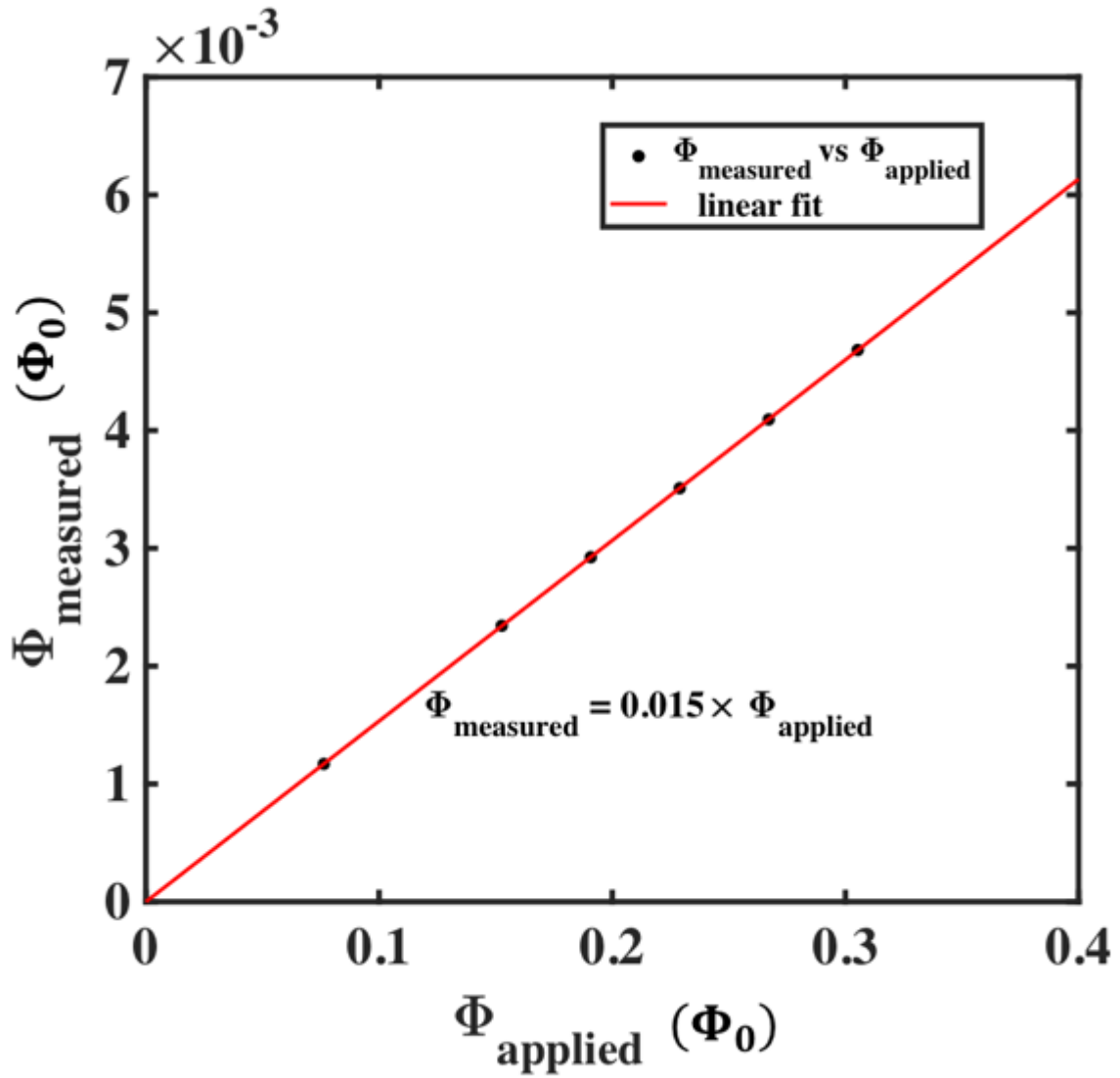
$$\sigma_\Phi^2 = \int_0^\infty S_\Phi(\omega) d\omega \quad (\text{M. 14})$$

E Calibration of MC Time Step

E.1 Inter-calibration of time scales

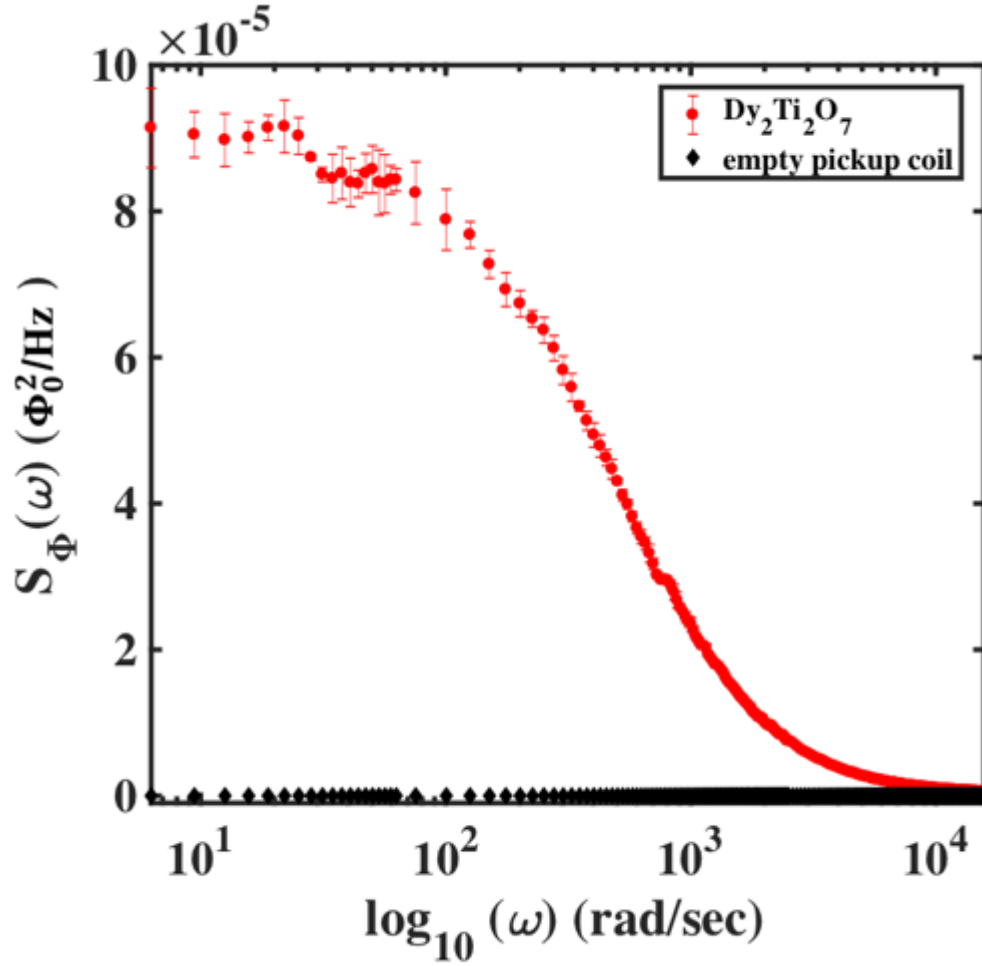
To obtain a correspondence between MC-step time and actual time, we assume that the MC temperature is equal to the measured temperature of the experiment in the range 1.2K to 3K. We then compare generation-recombination time constants obtained from fitting $S(\omega, T)$ to $\tau(T)/(1 + (\omega\tau(T))^b)$ for a. MC DSIM simulations in Fig. 2B to yield $\tau_{MC\ DSIM}(T)$, and b. experimental data in Fig. 3A to yield $\tau_{experiment}(T)$, respectively. The temperature T is used as the implicit variable. The slope of a linear fit of $\tau_{MC\ DSIM}(T)$ versus $\tau_{experiment}(T)$ yields the correspondence between MC-step and actual time. The result yields that in these simulations 1MC-step = 83 ± 11 microseconds which is then used throughout our studies. The possibility of some nonlinearity in the correspondence of our MC-step to seconds, for example as reported in other MC simulations (Takatsu *et al*, JPSJ 82, 104710 (2013)), will require future studies on how scaling the periodic boundary conditions and MC sample volumes impacts the usual linear correspondence used in similar experiment-MC comparisons (Ref. 10).

Supplementary Information Fig. 1



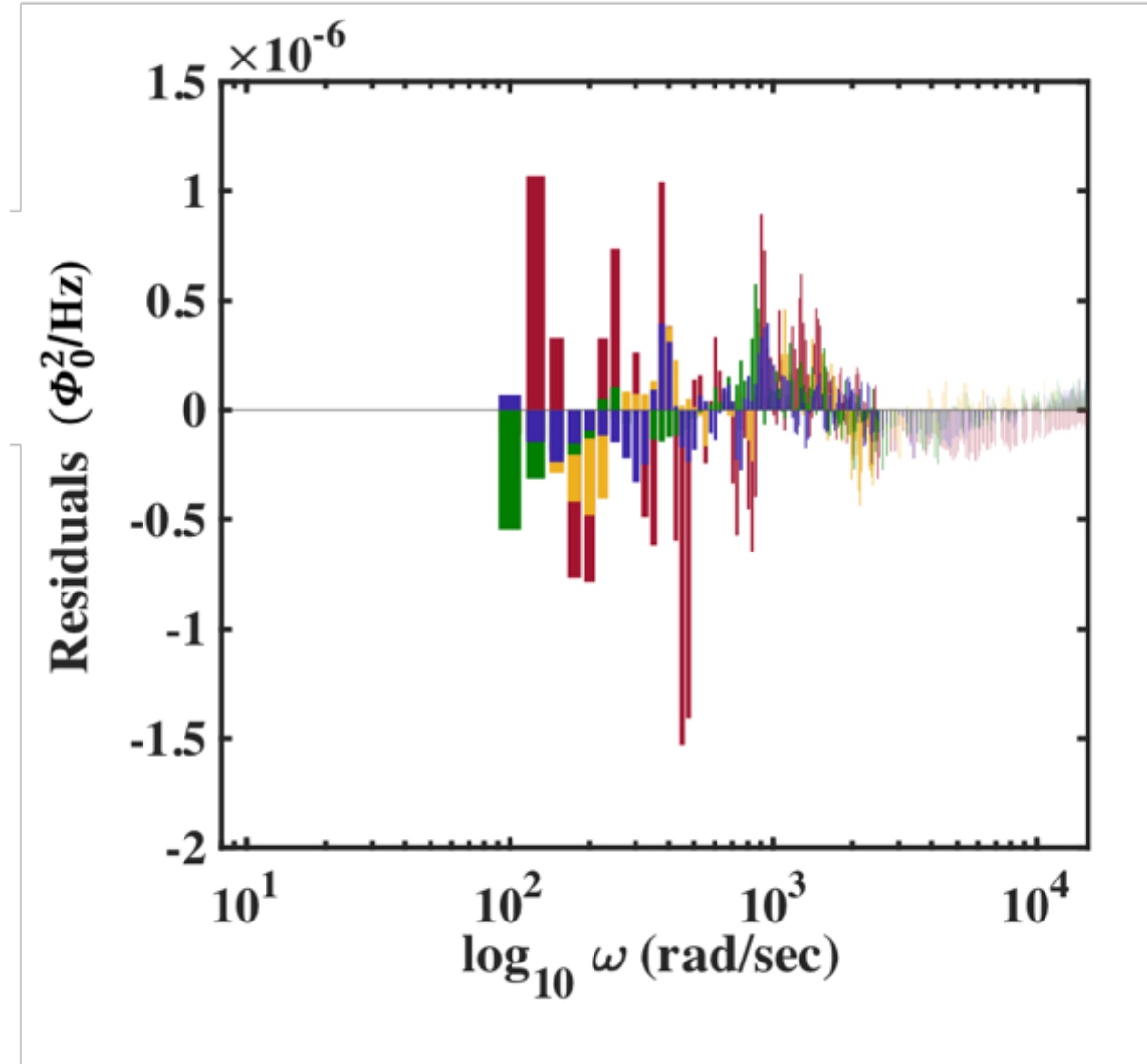
S.I. Figure 1: Here we show linear relationship between flux applied to the pickup coil via a drive coil and flux output by the SQUID. The slope between the two gives us the transfer function between the pickup coil and the SQUID.

Supplementary Information Fig. 2



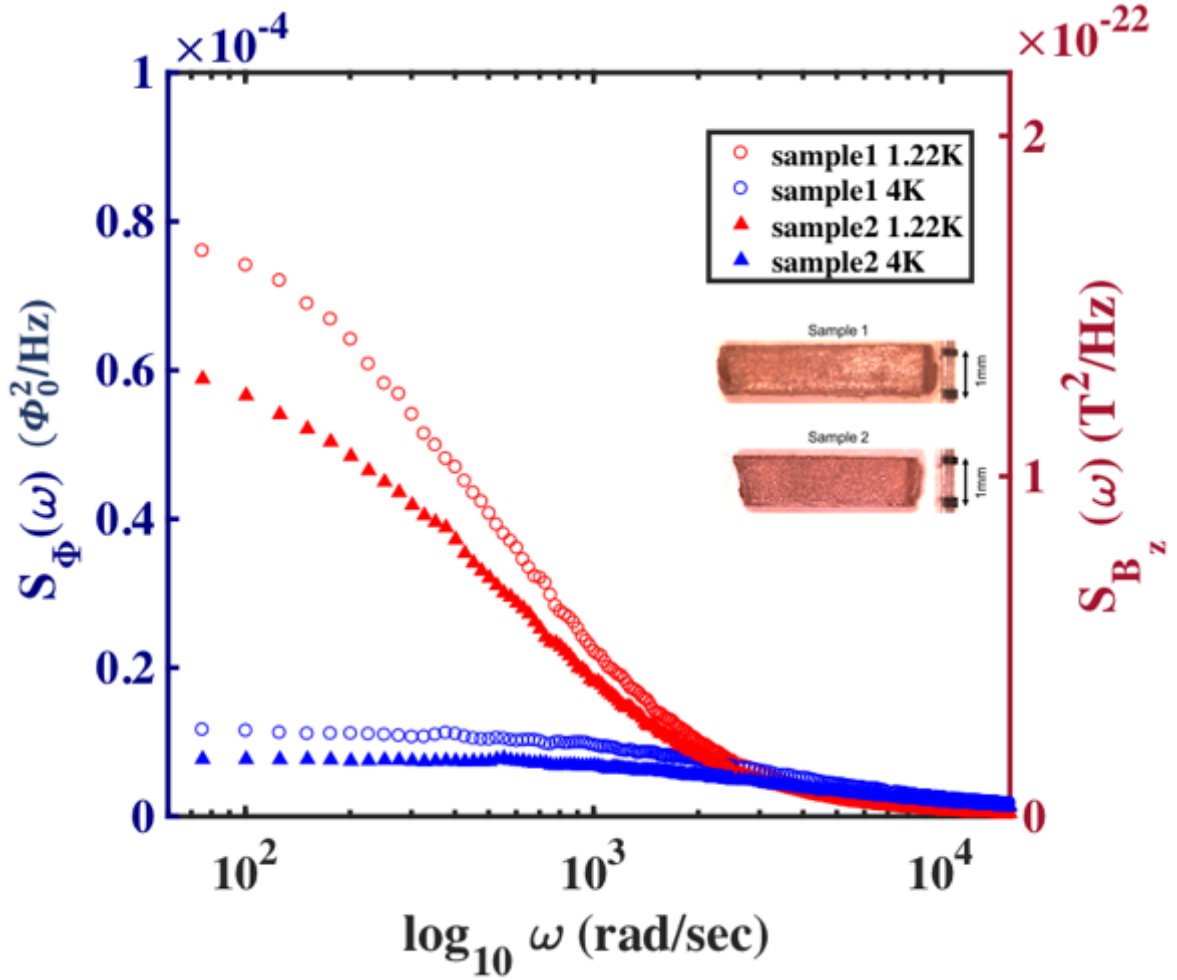
S.I. Figure 2: A typical spectrum of magnetic-flux noise spectral density detected from a sample of $\text{Dy}_2\text{Ti}_2\text{O}_7$ (at 1.22K) compared to flux-noise spectral density of empty pickup coil corresponding to $\sim 16.8 \times 10^{-12} \phi_0^2/\text{Hz}$. The black data points are only meaningfully visible because of a vertical shift in the position of 0.

Supplementary Information Fig. 3



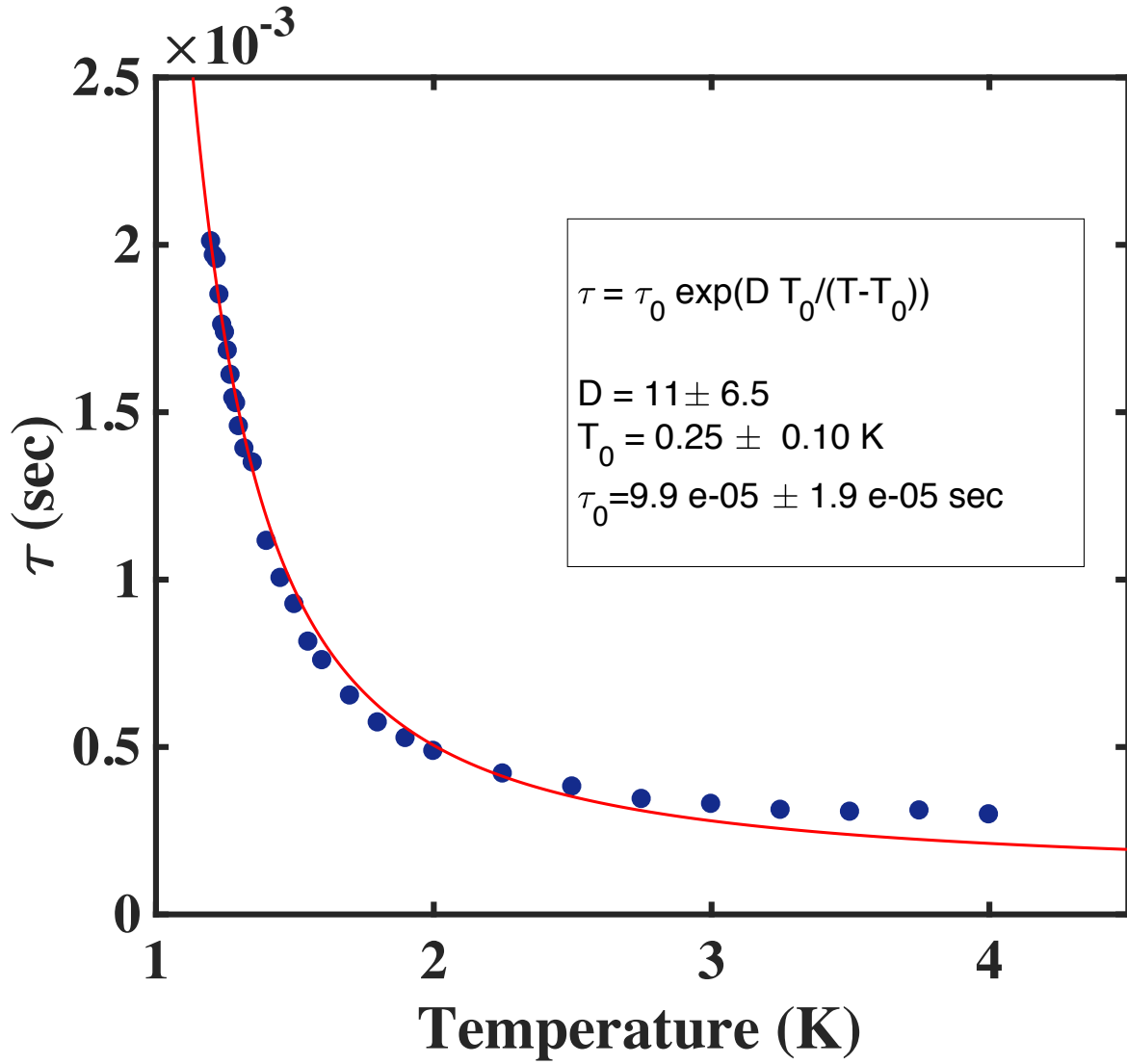
S.I. Figure 3: Residuals ($S_\phi(\omega, T) - S_{FIT}(\omega, T)$) for fits of measured flux noise spectral density (Fig. 3) to Eq. (5) are shown here for four temperatures. Here red points are for $T=1.2\text{K}$, yellow $T=2.0\text{K}$, green $T=3\text{K}$, blue $T=4\text{K}$

Supplementary Information Fig. 4



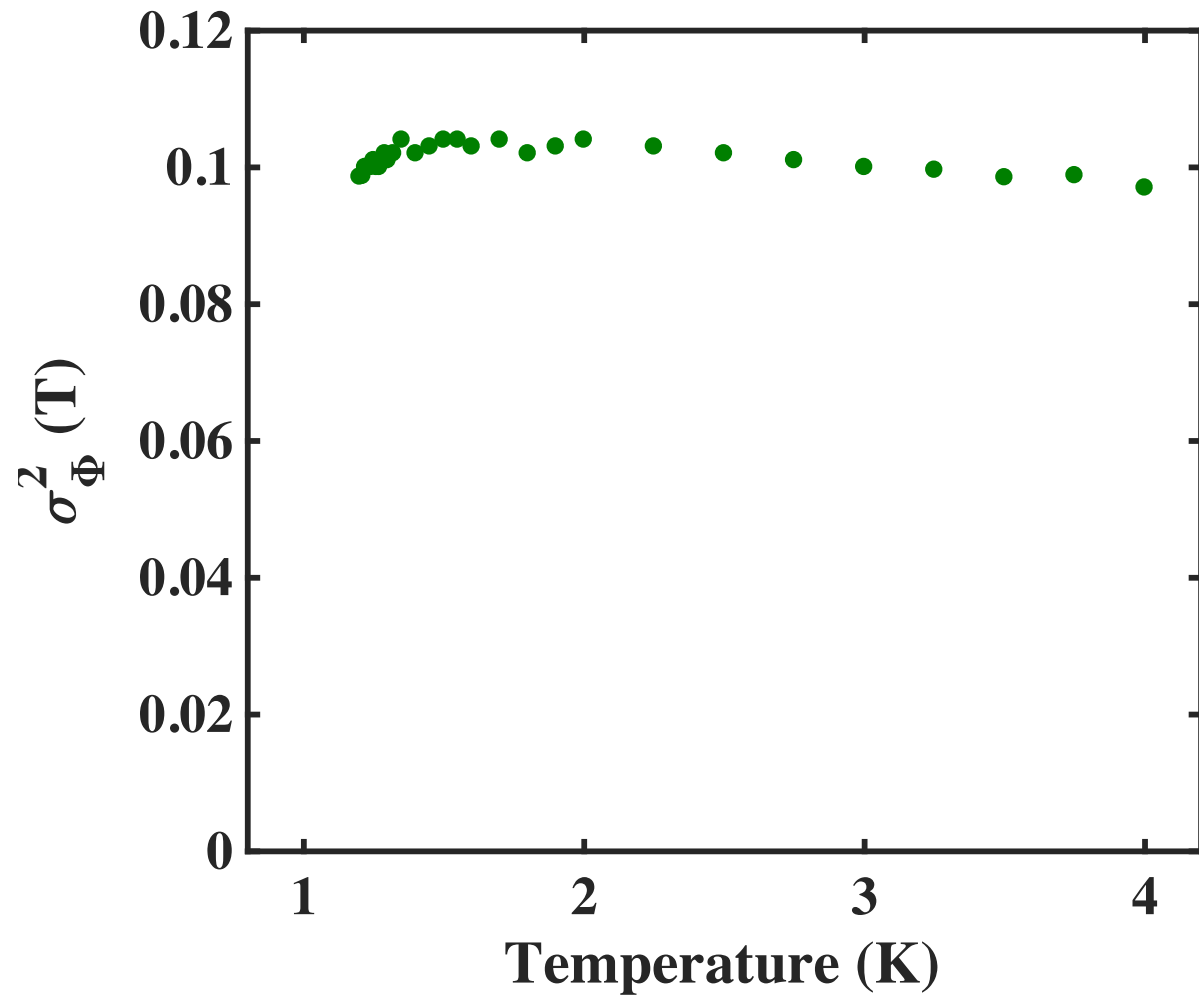
S.I. Figure 4: Plot of magnetic flux noise $S_\Phi(\omega, T)$ from two different $\text{Dy}_2\text{Ti}_2\text{O}_7$ rod shaped samples. We observe that the flux noise spectral density from two separate $\text{Dy}_2\text{Ti}_2\text{O}_7$ samples is very similar and therefore this experiment is quite repeatable on single crystals of $\text{Dy}_2\text{Ti}_2\text{O}_7$. The differences in magnitude and time constant are due to the geometrical differences between the two samples.

Supplementary Information Fig. 5



S.I. Figure 5: Plot of time constant from fits to measured $S_\phi(\omega, T)$ data as shown in Fig. 3. The flux-noise derived time constant behaves in a super Arrhenius fashion $\tau(T) = \tau_0 \exp\left(D \frac{T_0}{T - T_0}\right)$, consistent with previous measurements of this quantity from susceptibility experiments (Ref 27) which again exhibited super-Arrhenius time constant behavior with $\tau_0 \sim 1.4 \times 10^{-4} \text{ s}$, $D \approx 14$, $T_0 \approx 0.26 \text{ K}$.

Supplementary Information Fig. 6



S.I. Figure 6: Plot of measured variance of flux σ_{Φ}^2 shows that it is approximately constant as a function of temperature, in this range.

References

- 1 Dirac, P. Quantised Singularities in the Electromagnetic Field. *Proceedings of the Royal Society A: Mathematical, Physical and Engineering Sciences* 133, 60-72 (1931)
- 2 Hooft, G. Magnetic monopoles in unified gauge theories. *Nuclear Physics B* 79, 276-284 (1974)
- 3 Polyakov, A.M. Particle Spectrum in the Quantum Field Theory, *JETP Lett.* 20, 194 (1974).
- 4 Cabrera, B. First Results from a Superconductive Detector for Moving Magnetic Monopoles, *Phys. Rev. Lett.* 48, 1378 (1982)
- 5 Ryzhkin I. A. Magnetic relaxation of rare-earth pyrochlores, *JETP* 101, 481 (2005)
- 6 Castelnovo C., Moessner R., Sondhi S.L. Magnetic monopoles in spin ice, *Nature* 451, 42 (2008)
- 7 Klyuev, A., Ryzhkin, M. & Yakimov, A. Statistics of Fluctuations of Magnetic Monopole Concentration in Spin Ice. *Fluctuation and Noise Letters* 16, 1750035 (2017)
- 8 Kirschner, F.K.K., Flicker, F., Yacoby, A., Yao, N. & Blundell, S.J. Proposal for the detection of magnetic monopoles in spin ice via nanoscale magnetometry. *Physical Review B* 97, (2018)
- 9 Castelnovo, C., Moessner, R. & Sondhi, S. Spin Ice, Fractionalization, and Topological Order. *Annual Review of Condensed Matter Physics* 3, 35-55 (2012)
- 10 Jaubert, L. & Holdsworth, P. Magnetic monopole dynamics in spin ice. *Journal of Physics: Condensed Matter* 23, 164222 (2011)
- 11 Rosenkranz S. *et al* Crystal-field interaction in the pyrochlore magnet $\text{Ho}_2\text{Ti}_2\text{O}_7$. *Journal of Applied Physics* 87:5914-5916. (2000)
- 12 Ramirez, A., Hayashi, A., Cava, R., Siddharthan, R. & Shastry, B. Zero-point entropy in 'spin ice'. *Nature* 399, 333-335 (1999)

-
- 13 den Hertog B., Gingras M Dipolar Interactions and the Origin of Spin Ice in Ising Pyrochlore Magnets. *Phys. Rev. Lett.* 84: 3430. (2000)
 - 14 Kaiser V., *et al*, Emergent electrochemistry in spin ice: Debye-Hückel theory and beyond *Phys. Rev. B* 98, 144413 (2018)
 - 15 Burgess, R. E. The Statistics of Charge Carrier Fluctuations in Semiconductors. *Proc. Phys. Soc. B* 69 1020 (1956)
 - 16 van Vliet, K. M. and Fassett, J. R. Fluctuation Phenomena in Solids, edited by Burgess, R. E. *Academic Press, New York*(1965)
 - 17 Wilson, C. M. & Prober, D. E. Quasiparticle number fluctuations in superconductors. *Phys. Rev. B.* 69, 094524 (2004)
 - 18 Mitin V., Reggiani L., and Varani L. *Noise and Fluctuations Control in Electronic Devices*, Chapter 2, American Scientific Publishers (2002)
 - 19 Konczakowska A. and Wilamowski B.M. *Fundamentals of Industrial Electronics*, Chapter 11, Taylor & Francis (2011)
 - 20 Melko, R. G. and Gingras, M. J. P. Monte Carlo studies of the dipolar spin ice model *J. Phys.: Condens. Matter* 16 R1277 (2004)
 - 21 Vitale, S., Cavalleri, A., Cerdonio, M., Maraner, A. and Prodi, G.A., Thermal equilibrium noise with $1/f$ spectrum in a ferromagnetic alloy: Anomalous temperature dependence, *Journal of Applied Physics* 76, 6332 (1998).
 - 22 Reim, W., Koch, R., Malozemoff, A., Ketchen, M. & Maletta, H. Magnetic Equilibrium Noise in Spin-Glasses:Eu_{0.4}Sr_{0.6}S. *Physical Review Letters* 57, 905-908 (1986)
 - 23 Snyder, J. et al. Low-temperature spin freezing in the Dy₂Ti₂O₇ spin ice. *Phys. Rev. B.* 69 064414 (2004)
 - 24 Matsuhira, K. et al. Spin dynamics at very low temperature in spin ice Dy₂Ti₂O₇. *J. Phys. Soc. Jpn.* 80 123711 (2011)
 - 25 Yaraskavitch et al. Spin dynamics in the frozen state of the dipolar spin ice material Dy₂Ti₂O₇. *Phys. Rev. B.* 85, 020410 (2012)

-
- 26 Kassner, E. R. et al. Supercooled spin liquid state in the frustrated pyrochlore $\text{Dy}_2\text{Ti}_2\text{O}_7$. *Proc. Nat. Acad. Sci.* 112 8549 (2015)
- 27 Eyvazov, A. B. et al. Common glass-forming spin liquid state in the pyrochlore magnets $\text{Dy}_2\text{Ti}_2\text{O}_7$ and $\text{Ho}_2\text{Ti}_2\text{O}_7$. *Phys. Rev. B.* 98 214430 (2018)
- 28 Fennell, T. et al. Neutron scattering investigation of the spin ice state in $\text{Dy}_2\text{Ti}_2\text{O}_7$. *Phys. Rev. B.* 70 134408 (2004)
- 29 Quilliam, J. A., Meng, S., Mugford, C. G. A., Kycia, J. B., Evidence of Spin Glass Dynamics in Dilute $\text{LiHo}_x\text{Y}_{1-x}\text{F}_4$, *Phys. Rev. Lett.* 101, 187204 (2008)
- 30 Yau, L.D. and Sah, C-T., Theory and experiments of low-frequency generation-recombination noise in MOS transistors, *IEEE Transactions on Electron Devices* 16 170 - 177 (1969)
- 31 Morris D et al. Dirac Strings and Magnetic Monopoles in the Spin Ice $\text{Dy}_2\text{Ti}_2\text{O}_7$. *Science* **326**: 411-414 (2009)
- 32 Bramwell S. T. et al, Measurement of the charge and current of magnetic monopoles in spin ice, *Nature* **461**, 956–959 (2009)
- 33 Bovo L, Bloxson J, Prabhakaran D, Aeppli G, Bramwell S Brownian motion and quantum dynamics of magnetic monopoles in spin ice. *Nat. Comm.* 4:1535-1542. (2013)
- 34 Giblin S, Bramwell S, Holdsworth P, Prabhakaran D, Terry I Creation and measurement of long-lived magnetic monopole currents in spin ice. *Nat. Phys.*, 7:252-258. (2011)
- 35 Kaiser, V., Bramwell, S. T., Holdsworth, P. C. W., Moessner, R. ac Wien Effect in Spin Ice, Manifest in Nonlinear, Nonequilibrium Susceptibility. *Phys. Rev. Lett.* 115 037201 (2015)
- 36 Paulsen, C. et al. Experimental signature of the attractive Coulomb force between positive and negative magnetic monopoles in spin ice. *Nat. Phys.* 12 661 (2016)